Nanoscale

PAPER

View Article Online
View Journal | View Issue

Cite this: *Nanoscale*, 2015, **7**, 6667

Modulation of the electron transfer processes in Au–ZnO nanostructures†

M. E. Aguirre,[a] A. Armanelli,[a] G. Perelstein,[a] A. Feldhoff,[b] A. J. Tolley[c] and M. A. Grela*[a]

Received 17th January 2015,
Accepted 9th March 2015

DOI: 10.1039/c5nr00364d

www.rsc.org/nanoscale

Plasmonic nanostructures comprising Au and ZnO nanoparticles synthesized by the spontaneous reduction of $HAuCl_4$ in ethylene glycol were used to assess the possibility of modulating the direction of the electron transfer processes at the interface. One electron UV reduction and visible oxidation of the reversible couple TEMPOL/TEMPOL-H was confirmed by EPR spectroscopy. The apparent quantum yield for TEMPOL-H conversion under continuous wave visible excitation depends on the irradiation wavelength, being 0.57% and 0.27% at 450 ± 12 and 530 ± 12 nm, respectively. These results indicate that both the surface plasmon resonance and the interband transition from the 5d to the 6s level of Au nanoparticles contribute to the visible activity of the nanostructure. In addition, by detecting free electron conduction band electrons in ZnO, after the visible excitation of Au/ZnO nanostructures, we provide direct evidence of the photoexcited electron transfer from gold nanoparticles to ZnO.

Introduction

Photoinduced interfacial electron transfer is a key phenomenon which is central to molecular optoelectronics, energy conversion and catalysis.[1–5] Of particular interest is the question whether and to what extent hot-electron carriers created by surface plasmon excitation of metal nanoparticles can participate in charge transfer processes at the interface.[6] Small domains of metal nanoparticles in which the high energy carriers can rapidly reach the interface seem essential to the task.[7]

Current understanding of the dynamics of photoexcited gold nanoparticles indicates that after optical excitation hot electrons lose their energy in different processes having dissimilar time constants, which involve electron–electron scattering (100 fs), electron–phonon coupling (1–10 ps) and, ultimately, heat dissipation from the gold nanoparticle to the environment through phonon–phonon coupling (~100 ps).[8–11]

Chemical transformations of molecular adsorbates at metal surfaces induced by plasmon excitations are well known. It has been recognized that intense localized heating in the metal nanoparticles can trigger adsorbate reactions.[12–14] Besides, although sparse, hot-electron transfer into specific electronic states of molecules adsorbed on metal surfaces has proved to induce their dissociation.[15–19]

In metal-semiconductor nanostructures, charge separation following plasmon excitation may be favoured due to the injection of electrons into the conduction band of the semiconductor. The transfer of photoexcited electrons from a gold particle to the conduction band of titanium dioxide has been put forward by Tian and Tatsuma.[20,21] Their work demonstrates the development of anodic photocurrents on TiO_2 films loaded with Au nanoparticles, whose intensity correlates with the extinction spectrum of the nanostructure under visible irradiation and becomes inhibited in the presence of an acceptor (O_2) in solution. However, the clearest evidence of the electron transfer from gold NPs to the conduction band of TiO_2 was obtained by Furube and coworkers who observed a transient absorption of electrons in the conduction band of TiO_2 at 3440 nm after light absorption by the surface plasmon resonance band, SPR, of gold NPs.[22,23]

In this work, we present direct evidence that the direction of the photoinduced electron transfer processes in Au/ZnO nanostructures can be reverted from the semiconductor → metal to the metal → semiconductor direction, by changing the excitation wavelength from UV to visible. Although the conduction band positions of TiO_2 and ZnO are very similar, their electronic structure differs substantially. The conduction band of titanium dioxide basically consists of empty 3d Ti^{4+} orbitals, while that of ZnO mainly involves 4s orbitals of Zn^{2+}. This difference, in turn, affects not only the electron effective mass

[a]*Departamento de Química, Universidad Nacional de Mar del Plata, Funes 3350, B7602AYL Mar del Plata, Argentina. E-mail: magrela@mdp.edu.ar*
[b]*Institut für Physikalische Chemie und Elektrochemie, Leibniz Universität Hannover, Callinstraße 3a, D-30167 Hannover, Germany*
[c]*Centro Atómico Bariloche – R8400AGQ San Carlos de Bariloche, Río Negro, Argentina*

†Electronic supplementary information (ESI) available. See DOI: 10.1039/c5nr00364d

but also the density of states, ρ. Actually, considering that $\rho(TiO_2)/\rho(ZnO) \sim 200$[24] one would expect electronic coupling to be much more efficient in TiO_2 than in ZnO. Thus, it is not possible to anticipate whether or not in metal/ZnO nanostructures high energy electrons produced by metal excitation can be transferred to the conduction band of the semiconductor.[25]

Here we focus on the photoinduced changes in the oxidation states of a molecular probe 4-hydroxy-2,2,6,6-tetramethylpiperidine 1-oxyl, TEMPOL (I), and its hydroxylamine, TEMPOL-H (II). We observed direct evidence that (I) and (II) can be interconverted by selective UV irradiation of the semiconductor and the metal in the visible region.

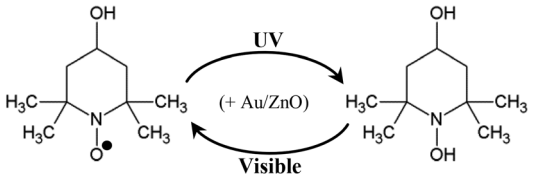

TEMPOL, (I) TEMPOL-H, (II) (1)

We hypothesize that under UV excitation of the semiconductor, the holes are scavenged by the solvent molecules, while the electrons are used to reduce TEMPOL to TEMPOL-H, however, under visible excitation the electrons are transferred to the oxide, and then used in oxygen reduction, while hydroxylamine replenishes the hole left in the metal, accounting for the TEMPOL regeneration.

The transfer of electrons in the Au to ZnO direction, after selective irradiation of the nanostructures in the visible region, was confirmed by direct observation of conduction band electrons in ZnO by EPR spectroscopy,[26–28] under anaerobic conditions. Thus, we definitively probe that by modulating the excitation wavelength the electron flow direction can be switched, which is interesting for the development of logical devices.

Experimental section

Materials

Hydrogen tetrachloroaurate trihydrate, 99.9%, (Aldrich), 4-hydroxy-2,2,6,6-tetramethylpiperidine 1-oxyl (Aldrich), zinc acetate dihydrate (Fluka), sodium hydroxide (Merck), tetramethylammonium hydroxide (Sigma) were of the highest available purity and used as received. Ethylene glycol (Biopack), 1-octanol (extra pure grade, Merck), ethyl acetate (Sintorgan), heptane (Sintorgan) and dimethylsulfoxide (chromatographic grade, Sintorgan) were used without further purification.

$KCr(NH_3)_2(NCS)_4$ was prepared from the Reinecke salt[29] (Aldrich) and recrystallized from warm water as described in ref. 29.

Methods

Synthesis of Au/ZnO nanostructures. ZnO nanoparticles were first prepared by alkaline hydrolysis/condensation reactions using zinc acetate as the precursor, following published procedures.[27] Briefly, 6.25 mL of a 550 mM solution of tetramethylammonium hydroxide in ethanol was slowly added to 20 mL of a 0.1 M solution of zinc acetate in dimethyl sulfoxide The reaction was stopped by precipitation of the nanocrystals with ethyl acetate, and repeatedly purified from the solvents and excess reagents by two cycles of heptane-induced precipitation, and resuspension in ethylene glycol.

Au/ZnO nanostructures were synthesized by the spontaneous room temperature reduction of $HAuCl_4$ in the presence of the as-prepared ZnO nanoparticles dispersed in neat ethylene glycol.[30]

Characterization

Optical absorption spectra of the Au/ZnO nanocomposites were recorded on an Agilent 8453 diode array spectrophotometer.

The crystalline properties of ZnO and Au/ZnO nanostructures were examined *via* powder X-ray diffraction (XRD) and by high resolution transmission electron microscopy (HRTEM). For details see ref. 30.

Electron paramagnetic resonance (EPR) experiments were performed at 298 K with a Bruker ELEXSYS E500 T spectrometer, operating at the X band. Amplitude signals were transformed in radical concentrations by comparing the area under the EPR absorption spectrum of the sample to that of a concentration standard of TEMPOL, recorded at the same microwave power, modulation amplitude, and amplification gain.[31]

Photolysis

To determine the interconversion between I and II, two different setups were used. In the first one, experiments were carried out by irradiating the samples in a square prismatic cell using a 150 W Osram Xe lamp, provided with a PTI 101 monochromator to isolate the bands at 303 ± 20, 450 ± 12 and 530 ± 12 nm. The former band was used to produce TEMPOL-H from TEMPOL. The regeneration of TEMPOL from its hydroxylamine was first explored using two long-pass glass filters (Schott GG-400 and GG-435) to prevent absorption of wavelengths shorter than λ = 435 nm and then carefully scrutinized by isolating the bands at 450 and 530 nm with the above mentioned monochromator. In the first setup, well determined volumes (20 μL) of the suspension were withdrawn from the cell and transferred to thin cylindrical silica EPR tubes in order to record the EPR spectrum. Alternatively, to minimize possible errors, the samples were directly irradiated in the EPR tubes using the same light sources.

For the detection of conduction band electrons by EPR spectroscopy, about 15 μL of concentrated samples of ZnO and Au/ZnO nanostructures dispersed in ethylene glycol were loaded in a sealable thin quartz tube. The samples were irradiated inside the EPR cavity during the irradiation with a 150 W Osram Xe lamp using the above mentioned Schott GG-400 and GG-435 long-pass glass filters.

Incident photon fluxes were determined using the Reinecke salt as actinometer.[29]

Results and discussion

We have recently shown that the reduction of $HAuCl_4$ by ethylene glycol in the presence of ZnO nanoparticles yields stable nanostructures in good electron contact.[30] In addition, the as synthesized materials show a relatively sharp visible peak at 535 nm, and negligible light scattering, see Fig. 1. Analysis by HRTEM demonstrated that the nanostructures consist of small ZnO nanoparticles (5.0 nm) in contact with bigger (15 nm) spherical Au nanoparticles.

TEMPOL ↔ TEMPOL-H interconversion

The EPR spectrum of TEMPOL shows the well-known three-line spectrum of a nitroxide (Fig. 2) resulting from ^{14}N hyperfine coupling (a_N), (curve b).[32,33] It is apparent that the heights of the peaks decrease at higher fields, a fact that is characteristic of anisotropic motion about the axis of the N–O bond, due to solvent viscosity.[33,34] As observed in the inset of Fig. 2, each line is widened by the contribution of the hydrogen hyperfine coupling constants, a_H, mainly arising from the equatorial methyl and methylene protons.[35] Unresolved hyperfine interactions alter the line width and line shape of the m = 0, 1 and −1 lines.

The experimental spectrum was simulated using the computational package Easyspin,[36,37] to derive the g factor, the hyperfine coupling constants and the rotational correlation time. See ESI† for details.

UV irradiation at 303 ± 10 nm of a sample of 10 μM nitroxide in ethyleneglycol in the presence of the Au/ZnO nanocomposite, ([Au] = 0.625 mM, [ZnO] = 8.1 mM) leads to the sudden disappearance of the paramagnetic signal, see upper panel of Fig. 3. It is apparent that TEMPOL can be either reduced to the corresponding hydroxylamine (II), or oxidized to the oxoammonium cation (III), as described by reactions (2) and (3):

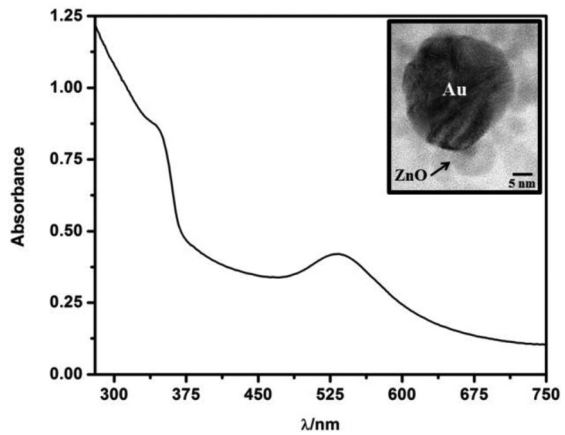

Fig. 1 UV-Vis spectrum of the Au/ZnO nanostructures dispersed in ethylene glycol. The nanocomposite was obtained by reduction of a 62 μM $HAuCl_4$ solution in ethylene glycol in the presence of ZnO ([ZnO] = 8.1 mM) see ref. 30. Inset: HRTEM showing contact between Au and ZnO.

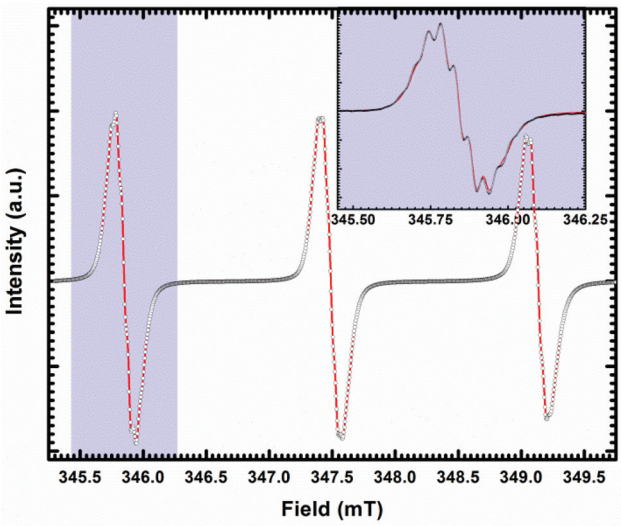

Fig. 2 Room temperature EPR spectra of degassed TEMPOL dissolved in ethylene glycol, hollow circles in black account for the experimental data. The red lines are the results of the simulation, see text. The inset shows the peak centered at 345.75 mT with higher resolution.

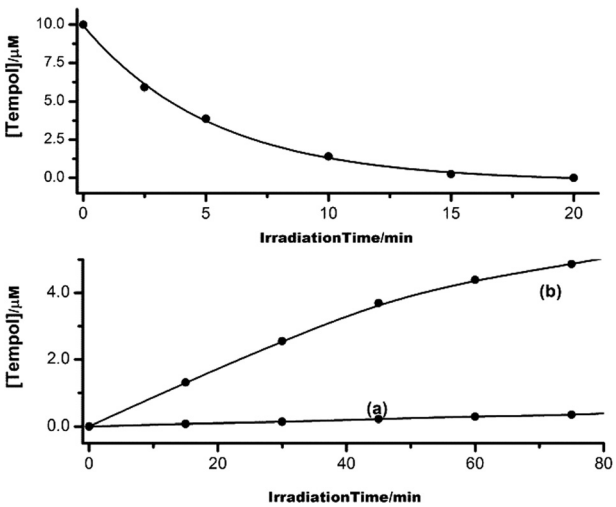

Fig. 3 Upper panel: decay of TEMPOL under UV irradiation. Lower panel: regeneration of TEMPOL in the dark (curve a) and under excitation of the nanostructures with wavelengths larger than 435 nm, (curve b).

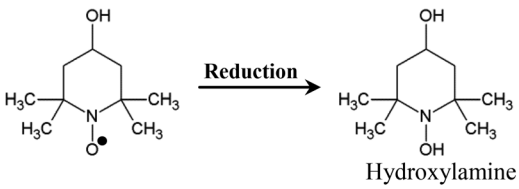

(2)

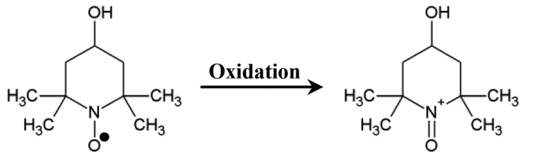

Oxoamonium cation (III) (3)

Considering that the concentration of TEMPOL ([TEMPOL] = 10 μM) is much lower than that of ethylene glycol ([EG] = 17.8 M) and that the oxidation of TEMPOL ($E^0_{(III/I)}$ = 0.81 V)[38] would probably occur in the inverted Marcus region,[39,40] the decay of the paramagnetic signal is ascribed to its reduction to hydroxylamine, and not to its conversion to the oxoammonium cation. This assumption is confirmed by observing that the paramagnetic signal is slowly regenerated by bubbling O_2 in the dark. This fact is taken as a proof that, under UV irradiation of the nanocomposite, the most important fate of the nitroxide is its reduction, while ethylene glycol, D, acts as the donor, as described by eqn (4)–(10) below.

$$Au/ZnO + h\nu_{(303\pm10\ nm)} \rightarrow Au/ZnO(e_{CB}^-, h_{VB}^+) \quad (4)$$

$$h_{VB}^+(ZnO) + D \rightarrow D^{\bullet+} \quad (5)$$

$$e_{CB}^-(ZnO) \rightarrow e^-(Au) \quad (6)$$

$$[e_{CB}^-(ZnO), (e^-(Au)] + O_2 \rightarrow O_2^{\bullet-} \quad (7)$$

$$TEMPOL + e_{CB}^- + H^+ \rightarrow TEMPOL\text{-}H \quad (8)$$

$$TEMPOL + e^-(Au) + H^+ \rightarrow TEMPOL\text{-}H \quad (9)$$

$$TEMPOL + O_2^{\bullet-} + H^+ \rightarrow TEMPOL\text{-}H + O_2 \quad (10)$$

TEMPOL reduction may be mediated by either conduction band ZnO electrons directly, reaction (8), by electrons transferred to the metal, reactions (6) + (9), or through the formation of superoxide radicals formed upon oxygen reduction, reactions (7) + (10). The above experiments do not provide any evidence to discriminate which mechanism prevails, but we will address this issue later. It is also interesting to recall that by monitoring the UV-Vis spectra of pure ZnO and Au/ZnO nanostructures, we have recently demonstrated the effective transfer of electrons in the ZnO → Au direction. Accordingly, we found that under UV irradiation, the excitonic band of ZnO progressively shifts to the blue until it reaches a steady state. However the irradiation of the Au/ZnO nanostructures under the same conditions, additionally results in a shift of the plasmon band from 535 to 520 nm (see Fig. 5 of ref. 30). This experiment unequivocally demonstrates the increased electron density in the metal, and can be taken as strong evidence that the junction between ZnO and Au nanoparticles in the nanostructure allows the transfer of electrons across the interface.

The reversible nature of the couple I/II lead us to envisage that this system is adequate to analyze the direction of the electron transfer process by changing the excitation wavelength. Thus, in an exploratory experiment, after the complete disappearance of TEMPOL we exposed the sample to visible irradiation, $\lambda > 435$ nm.

The result is shown in the lower panel of Fig. 3, curve b, and indicates that TEMPOL is regenerated at a rate substantially different than that observed in the dark.

In addition, we carefully examine the EPR spectrum of TEMPOL after its regeneration under visible irradiation, *i.e.*, in the presence of Au/ZnO nanostructures.

Our aim was to explore possible differences in the coupling constants and the rotational mobility of TEMPOL due to the interaction with the semiconductor and/or metal components of the nanocomposite. As it is known, nitroxides are commonly used as spin labels due to their stability and sensitivity of their spectra to the chemical environment. Experimental results are presented in Fig. 4 for the $m = -1$ peak.

Again, the spectra were simulated with the Easyspin,[36,37] program. We observe that the derived mean correlation time slightly changes from 1.82 ns to 1.62 ns on going from the spectrum taken in pure ethylene glycol to that determined in the presence of the nanocomposites dispersed in the same solvent. The details of the simulation and other differences in the spectra are summarized in the ESI.† Although the differences are not very significant, the decrease in the correlation time is consistent with the nitroxide interaction with the nanocomposite surface.

To gain additional insight, we take the spectrum of TEMPOL in an 8 mM sol of pure ZnO nanoparticles, *i.e.*, before Au loading. See Fig. 5.

It is apparent that the *g*-factor of TEMPOL in the 8 mM sol of ZnO nanoparticles is clearly distinguishable from that obtained either in the presence or absence of Au/ZnO nanostructures. Also the simulations indicate that the mean correlation time in this case is 3.52 ns, nearly a factor twice higher than that obtained for free TEMPOL. This is taken as evidence that the presence of gold in Au/ZnO nanostructures, somewhat impedes the interaction of ZnO with TEMPOL. Notice that

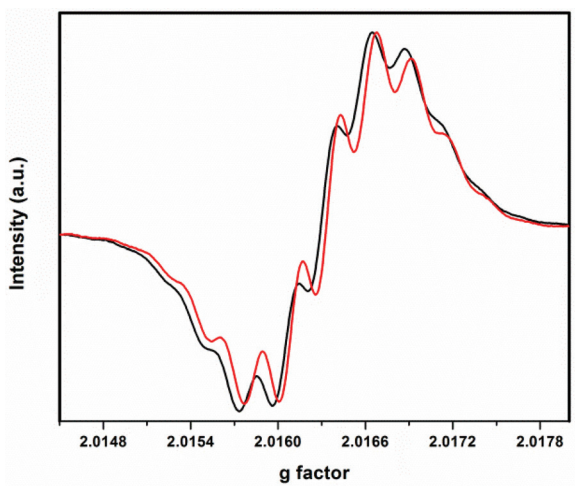

Fig. 4 Comparison between the room temperature EPR spectra of degassed TEMPOL dissolved in ethylene glycol. The black and red lines in the spectra obtained in the absence and presence of Au/ZnO nanostructures.

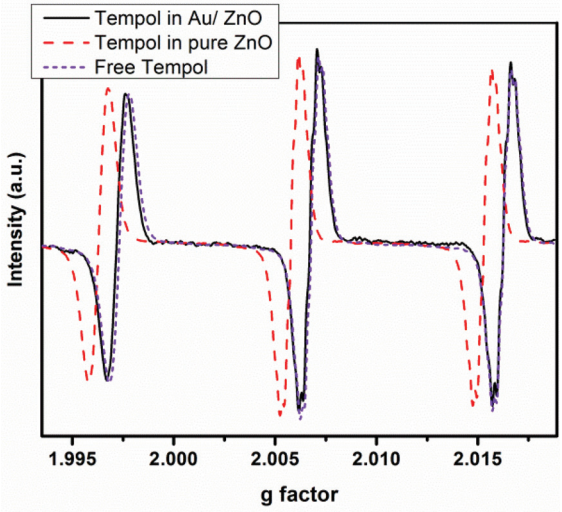

Fig. 5 Comparison between the experimental degassed spectrum of free TEMPOL with those obtained in the presence of ZnO and Au/ZnO nanostructure. The spectrum obtained in the presence of ZnO is clearly different from the others, revealing the interaction of the TEMPOL with the semiconductor surface, see text.

while the correlation time is derived from a simulation procedure, the *g* factor is a direct experimental parameter. This last result indicates a different environment of the radical. Thus, the experimental evidence points to discarding the ZnO surface as the reactive interface of our studies. This may be indicative of the fact that the reduction of TEMPOL under UV irradiation should be accounted for by reactions (6) + (9) or (7) + (10), rather than by reaction (8). On the other hand, one may be tempted to ascribe the oxidation of the hydroxylamine to a Au–hole replenish process after the excitation of the plasmon band, according to the successive elementary steps represented by reactions (11)–(14).

The above mechanism explains TEMPOL regeneration by considering that the oscillation of the plasmon band represented by reaction (11), leads to the transfer of an electron in the metal → semiconductor direction, reaction (12), leaving a hole in the Au surface, which is able to oxidize TEMPOL-H, reaction (13), while electrons in ZnO surface are depleted by their reaction with oxygen, reaction (14).

It is worthwhile to say that, in order to confirm the role of O_2 as an electron scavenger, a control experiment was performed, as described below. In this run, the sample was irradiated by UV light to deplete the signal of TEMPOL. After this procedure air was eliminated by freezing and pumping and the sample was fully irradiated inside the EPR cavity at wavelengths larger than 435 nm for 90 min. During this period, no signal of TEMPOL could be observed, confirming the mechanism proposed by reactions (10)–(14).

$$\mathrm{Au/ZnO} + h\nu_{(\mathrm{Visible})} \rightarrow \mathrm{Au}(\delta_+, \delta_-)/\mathrm{ZnO} \quad (11)$$

$$\mathrm{Au}(\delta_+, \delta_-)/\mathrm{ZnO} \rightarrow \mathrm{h^+(Au)/ZnO}(\mathrm{e_{CB}}^-) \quad (12)$$

$$\mathrm{h^+(Au)} + \mathrm{TEMPOL\text{-}H} \rightarrow \mathrm{TEMPOL} + \mathrm{H^+} \quad (13)$$

$$\mathrm{e_{CB}}^- + \mathrm{O_2} \rightarrow \mathrm{O_2}^{\bullet -} \quad (14)$$

The experiment shown in the lower panel of Fig. 3 was performed by polychromatic visible excitation of the nanostructures at wavelengths larger than 435 nm. Although chemical transformations induced by visible irradiation are often assigned to the excitation of the plasmon band, it should be stressed that by irradiating at wavelengths higher than 400 nm, one not only induces the oscillation of the 6s valence band electrons, but also facilitates the promotion of the electrons from the 5d to 6s levels of Au nanoparticles.[41] At variance with the behaviour observed for Ag, the SPR band and the interband transitions in Au nanoparticles are partially overlapped.[41] It is also apparent that interband transitions dominate the absorption of the metal nanoparticles for wavelengths shorter than 475 nm,[41] a fact that has been recognized in very few cases in the reports on plasmonic photocatalysis.[42–44]

Thus, quantitative experiments were performed to evaluate the amount of TEMPOL regenerated as a function of the irradiation time by exciting the samples at 450 ± 12 and 530 ± 12 nm. Results are shown in Fig. 6. As already stated the 530 and 450 bands were selected because at the former wavelength the extinction spectrum of Au nanoparticles is dominated by the oscillation of 6s electrons, while at 450 nm both, the SPR and the electronic excitation from the 5d to 6s levels are operative.

By combining the data shown in Fig. 6, with an independent estimation of the incident photon flux in each experiment we estimated the apparent quantum yields for the photoinduced TEMPOL regeneration. Results are summarized in Table 1. It should be stressed that in the absence of irradiation the rate of TEMPOL regeneration was not measurable.

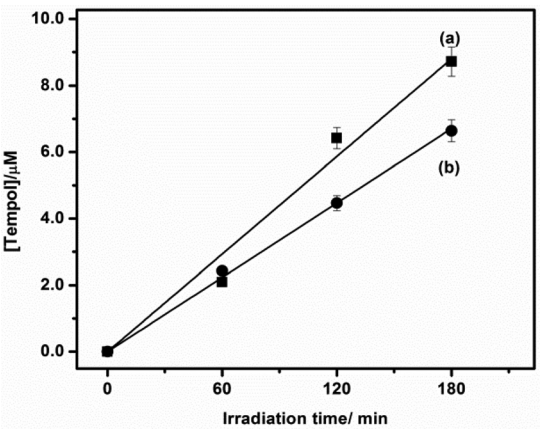

Fig. 6 Regeneration of TEMPOL and under excitation of the nanostructures with wavelengths at 450 and 530 nm, curves a and b, respectively.

Table 1 Apparent quantum yields for TEMPOL regeneration from TEMPOL-H obtained under visible irradiation of the Au/ZnO nanostructures

λ/nm	v^a/nM s^{-1}	ξ^b (%)
530 ± 12	0.553	0.27
450 ± 12	0.873	0.57

[a] Rate of TEMPOL regeneration obtained from the data in Fig. 6 at 450 and 530 nm. The incident photon fluxes at 450 and 530 nm are, respectively, 121 and 186 nM s^{-1}. [b] Apparent efficiencies defined as the ratio between v and the incident photon flux.

The data obtained above indicate that at 450 nm the apparent efficiency is near a factor 2.1 higher than at 530 nm, a fact that points to a substantial contribution of the interband transitions at the former wavelength.

To our knowledge there is no data to compare our results, however it is worthwhile to notice that Ohtani and coworkers have found that the action spectra of Au/TiO_2 are almost coincident with the total absorption spectra of the nanocomposites, which comprise the SPR as well as the interband transition.[45]

Below, we describe the experiments that allowed us to monitor the presence of conduction band electrons in ZnO under visible excitation of the nanostructures. In this way we were able to confirm the mechanism indicated by eqn (11)–(14).

Does the transfer of electrons from Au to ZnO actually account for the visible activity of Au/ZnO nanostructures?

To answer the above question, we designed an experiment which could be used to sense the presence of electrons in ZnO after the visible excitation of the nanostructures.

Gamelin and co-workers have thoroughly analyzed the EPR signature of conduction band electrons in colloidal ZnO quantum dots under accumulation conditions caused by the anaerobic irradiation of the semiconductor.[46] By combining NIR and EPR measurements they unequivocally ascribed the signal at $g \sim 1.96$ to free conduction band electrons.

Thus, about 15 μL of concentrated samples of ZnO and Au/ZnO nanostructures dispersed in ethylene glycol were loaded in sealable thin quartz tubes and examined by EPR spectroscopy, in the dark and under visible irradiation in anaerobic conditions. The results are represented in Fig. 7.

ZnO samples before Au deposition do not show any paramagnetic signal in the dark, indicating a probably low concentration of defects. In fact, different EPR signals with g-factors near 2.01, 1.96 and 1.97, have previously been detected and assigned to oxygen vacancies, Zn interstitials, and hydrogen interstitials, respectively.[47–49]

However, a different behaviour was found for the synthesized Au/ZnO nanostructures in the dark, which showed a small feature at $g = 1.9655$, as shown in curve (b) of Fig. 7.

We assign the new signal to the presence of free electrons in the conduction band that result from the charge transfer process taking place during the synthesis of the nanostructures until the building blocks attain the new Fermi energy level.[50]

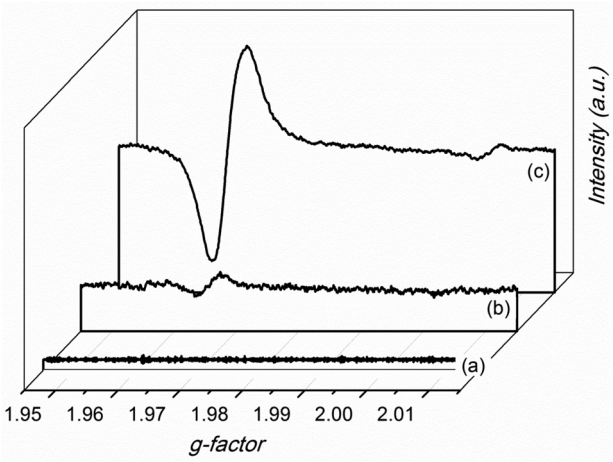

Fig. 7 Room temperature EPR spectra of as-prepared ZnO nanoparticles suspended in ethylene glycol (a), and Au/ZnO nanoparticles before (b), and during continuous irradiation at wavelengths longer than 435 nm (c).

The transfer of electrons occurs in the direction Au → ZnO because of the larger work function of the semiconductor and is also noticeable by XPS analysis which shows that the binding energy of Au 4f in the nanocomposite sample is higher than the value of reference for bulk Au°, in line with the proposed reduction of the electron density in gold nanoparticles.[51,52]

Curve (c) in Fig. 7 shows that visible irradiation ($\lambda >$ 435 nm) of the sample leads to a sudden outstanding increase of the singlet at $g \sim 1.96$ (which is now centred at $g = 1.9623$, *i.e.*, shifted to higher fields with respect to the signal obtained in the dark). It is worth noticing that the signal intensity remains stable during prolonged (1 hour) continuous visible excitation and, also, no noticeable changes could be detected in the spectrum after interrupting the irradiation (during a comparable period of time). It is interesting to recall that the Gamelin studies also reveal a size-dependence of the g-factor in the range $1.960 < g < 1.968$ for quantum dots with diameters between 3.0 and 7.0 nm. Also, for a given nanoparticle diameter, g values increase with $\langle n \rangle$, the average number of electrons per ZnO nanocrystal.[26,27] Taking into account the combined facts we considered that the change from $g = 1.9655$ to 1.9623, that occurs as a result of the irradiation process, reflects that the number of electrons per particle is low, and that they preferentially reside in larger sized particles which favour electron delocalization.[24] Irradiated samples also show the emergence of a weak signal centred at $g = 2.0045$. By double integration of the digitalized first-derivative EPR signals we estimate that the number of spins that contribute to this signal is about 40 times lower than those ascribed to CB electrons in ZnO. On the other hand, the g value of this signal is very close to that of the free electron ($g_e = 2.0023$) and

can be assigned to an organic radical derived from solvent oxidation.[47]

We have also observed a moderate enhancement of the signal at $g \sim 1.96$, by selectively irradiating the sample with blue and green leds, results not shown for simplicity. The lower intensity is accounted by the decrease in the photon flux in comparison with the polychromatic experiment.

Although the photoinduced charge transfer mechanism in the metal to semiconductor direction has been assessed in TiO_2 films loaded with Au nanoparticles, to our knowledge, no related evidence existed up to this moment for zinc oxide.

Conclusions

By analyzing the fate of the TEMPOL/TEMPOL-H redox couple we showed that ZnO/Au nanostructures can be used to modulate the direction of the electron transfer process at the Au–ZnO interface. The population of the ZnO conduction band under continuous, low power, visible excitation of the nanostructure, unequivocally proved in this work, is of practical interest for photocatalysis and is also relevant for the understanding of plasmon photoinduced charge-transfer processes at the metal–semiconductor interface.

Acknowledgements

This work was financially supported by the National Research Council of Argentina, CONICET, PIP 467, and ANPCyT PICT-2013-1456. MEA thanks CONICET for a doctoral fellowship.

References

1 L. Gundlach, B. Burfeindt, J. Mahrt and F. Willig, *Chem. Phys. Lett.*, 2012, **545**, 35–39.
2 R. Jiang, B. Li, C. Fang and J. Wang, *Adv. Mater.*, 2014, **26**, 5274–5309.
3 A. P. de Silva, *Phys. Chem. Lett.*, 2012, **2**, 2865–2871.
4 C. D. Lindstrom and X. Y. Zhu, *Chem. Rev.*, 2006, **106**, 4281–4300.
5 P. V. Kamat, *J. Phys. Chem. Lett.*, 2012, **3**, 663–672.
6 P. K. Jain, X. Huang, I. H. El-Sayed and M. A. El-Sayed, *Acc. Chem. Res.*, 2008, **41**, 1578–1586.
7 P. V. Kamat, *J. Phys. Chem. B*, 2002, **106**, 7729–7744.
8 T. S. Ahmadi, S. L. Logunov and M. A. El-Sayed, *J. Phys. Chem.*, 1996, **100**, 8053–8056.
9 P. K. Jain, W. Qian and M. A. El-Sayed, *J. Phys. Chem. B*, 2005, **110**, 136–142.
10 S. Link, A. Furube, M. B. Mohamed, T. Asahi, H. Masuhara and M. A. El-Sayed, *J. Phys. Chem. B*, 2002, **106**, 945–955.
11 G. V. Hartland, *Chem. Rev.*, 2011, **111**, 3858–3887.
12 J. C. Scaiano and K. J. Stamplecoskie, *Phys. Chem. Lett.*, 2013, **4**, 1177–1187.
13 C. Fasciani, C. J. Bueno Alejo, M. Grenier, J. C. Netto-Ferreira and J. C. Scaiano, *Org. Lett.*, 2011, **13**, 204–207.
14 M. Sun and H. Xu, *Small*, 2012, **8**, 2777–2786.
15 K. Watanabe, D. Menzel, N. Nilius and H.-J. Freund, *Chem. Rev.*, 2006, **106**, 4301–4320.
16 K. O. Aruda, M. Tagliazucchi, C. M. Sweeney, D. C. Hannah and E. A. Weiss, *Phys. Chem. Chem. Phys.*, 2013, **15**, 7441–7449.
17 C. Bauer, J.-P. Abid and H. H. Girault, *J. Phys. Chem. B*, 2006, **110**, 4519–4523.
18 K. O. Aruda, M. Tagliazucchi, C. M. Sweeney, D. C. Hannah, G. C. Schatz and E. A. Weiss, *Proc. Natl. Acad. Sci. U. S. A.*, 2013, **110**, 4212–4217.
19 S. Mukherjee, F. Libisch, N. Large, O. Neumann, L. V. Brown, J. Cheng, J. B. Lassiter, E. A. Carter, P. Nordlander and N. J. Halas, *Nano Lett.*, 2013, **13**, 240–247.
20 N. Sakai, Y. Fujiwara, Y. Takahashi and T. Tatsuma, *ChemPhysChem*, 2009, **10**, 766–769.
21 Y. Tian and T. Tatsuma, *J. Am. Chem. Soc.*, 2005, **127**, 7632–7637.
22 A. Furube, L. Du, K. Hara, R. Katoh and M. Tachiya, *J. Am. Chem. Soc.*, 2007, **129**, 14852–14853.
23 L. Du, A. Furube, K. Yamamoto, K. Hara, R. Katoh and M. Tachiya, *J. Phys. Chem. C*, 2009, **113**, 6454–6462.
24 J. B. Asbury, E. Hao, Y. Wang, H. N. Ghosh and T. Lian, *J. Phys. Chem. B*, 2001, **105**, 4545–4557.
25 L. Du, A. Furube, K. Hara, R. Katoh and M. Tachiya, *J. Photochem. Photobiol., C*, 2013, **15**, 21–30.
26 W. K. Liu, K. M. Whitaker, K. R. Kittilstved and D. R. Gamelin, *J. Am. Chem. Soc.*, 2006, **128**, 3910–3911.
27 R. Hayoun, K. M. Whitaker, D. R. Gamelin and J. M. Mayer, *J. Am. Chem. Soc.*, 2011, **133**, 4228–4231.
28 W. K. Liu, K. M. Whitaker, A. L. Smith, K. R. Kittilstved, B. H. Robinson and D. R. Gamelin, *Phys. Rev. Lett.*, 2007, **98**, 186804.
29 E. E. Wegner and A. W. Adamson, *J. Am. Chem. Soc.*, 1966, **88**, 394–404.
30 M. E. Aguirre, G. Perelstein, A. Feldhoff, A. Condó, A. J. Tolley and M. A. Grela, *New J. Chem.*, 2015, **39**, 909–914.
31 Y. Di Iorio, M. E. Aguirre, M. A. Brusa and M. A. Grela, *J. Phys. Chem. C*, 2012, **116**, 9646–9652.
32 C. C. Whisnant, S. Ferguson and D. B. Chesnut, *J. Phys. Chem.*, 1974, **78**, 1410–1415.
33 J. J. Windle, *J. Magn. Reson.*, 1981, **45**, 432–439.
34 P. F. Schwarz, N. J. Turro, S. H. Bossmann, A. M. Braun, A.-M. A. A. Wahab and H. Dürr, *J. Phys. Chem. B*, 1997, **101**, 7127–7134.
35 Y. Nosaka, H. Natsui, M. Sasagawa and A. Y. Nosaka, *J. Phys. Chem. B*, 2006, **110**, 12993–12999.
36 S. Stoll and A. Schweiger, *J. Magn. Reson.*, 2006, **178**, 42–55.
37 S. Stoll and A. Schweiger, *Biol. Magn. Reson.*, 2007, **27**, 299–321.
38 M. C. Krishna, D. A. Grahame, A. Samuni, J. B. Mitchell and A. Russo, *Proc. Natl. Acad. Sci. U. S. A.*, 1992, **89**, 5537–5541.

39 M. A. Grela and A. J. Colussi, *J. Phys. Chem. B*, 1999, **103**, 2614–2619.
40 M. A. Grela, M. A. Brusa and A. J. Colussi, *J. Phys. Chem. B*, 1999, **103**, 6400–6402.
41 M. A. Garcia, *J. Phys. D: Appl. Phys.*, 2011, **44**, 283001–283021.
42 W. Hou, W. H. Hung, P. Pavaskar, A. Goeppert, M. Aykol and S. B. Cronin, *ACS Catal.*, 2011, **1**, 929–936.
43 H. Zhu, X. Chen, Z. Zheng, X. Ke, E. Jaatinen, J. Zhao, C. Guo, T. Xie and D. Wang, *Chem. Commun.*, 2009, 7524–7526.
44 S.-i. Naya, A. Inoue and H. Tada, *ChemPhysChem*, 2011, **12**, 2719–2723.
45 E. Kowalska, O. O. P. Mahaney, R. Abe and B. Ohtani, *Phys. Chem. Chem. Phys.*, 2010, **12**, 2344–2355.
46 K. M. Whitaker, S. T. Ochsenbein, V. Z. Polinger and D. R. Gamelin, *J. Phys. Chem. C*, 2008, **112**, 14331–14335.
47 H. Zeng, G. Duan, Y. Li, S. Yang, X. Xu and W. Cai, *Adv. Funct. Mater.*, 2010, **20**, 561–572.
48 A. Janotti and C. G. Van de Walle, *Phys. Rev. B: Condens. Matter*, 2007, **76**, 165202.
49 J. r. J. Schneider, R. C. Hoffmann, J. r. Engstler, A. Klyszcz, E. Erdem, P. Jakes, R. d.-A. Eichel, L. Pitta-Bauermann and J. Bill, *Chem. Mater.*, 2010, **22**, 2203–2212.
50 M. E. Aguirre, G. Custo, M. Goes, P. Bueno, G. Zampieri and M. A. Grela, *J. Phys. Chem. C*, 2014, **118**, 2018–2027.
51 M.-K. Lee, T. G. Kim, W. Kim and Y.-M. Sung, *J. Phys. Chem. C*, 2008, **112**, 10079–10082.
52 Y. Zheng, L. Zheng, Y. Zhan, X. Lin, Q. Zheng and K. Wei, *Inorg. Chem.*, 2007, **46**, 6980–6986.